

Anionic Homopolymers Efficiently Target Zerovalent Iron Particles to Hydrophobic Contaminants in Sand Columns

ELIZABETH J. BISHOP,
DANIEL E. FOWLER,
JOANNA M. SKLUZACEK,
ELIZABETH SEIBEL, AND
THOMAS E. MALLOUK*

Department of Chemistry, The Pennsylvania State University,
University Park, Pennsylvania 16802, United States

Received May 23, 2010. Revised manuscript received
October 23, 2010. Accepted October 27, 2010.

The transport of microscale carbonyl iron powder suspensions modified with anionic homopolymers was studied in water-saturated sand columns containing well-dispersed hydrophobic sand grains. Sand grains functionalized with hexadecyltrimethoxysilane were coated with a eutectic mixture of dichlorobenzenes that was solid at $-10\text{ }^{\circ}\text{C}$ and was mixed by grinding with unmodified sand grains. The dichlorobenzene coating liquefied at the temperature of the transport experiments, and the coated grains were thus mimetic of uniform droplets of dense nonaqueous phase liquid (DNAPL) contaminants. By comparing iron particle transport in uncontaminated columns with those that contained a small fraction of DNAPL-coated sand grains, sticking coefficients for both types of grains could be estimated. The anionic polyelectrolytes tested (polyacrylate, carboxymethylcellulose, alginate, and metasilicate) all gave low particle sticking coefficients (0.004–0.05) to unmodified sand, as expected from earlier studies. However, iron particles modified with the two moderately hydrophobic polymers (carboxymethylcellulose and polyacrylate) had 30-fold higher sticking coefficients (0.40 and 0.13, respectively) to the model DNAPL surface than they did to the sand surface. In contrast, no significant difference between the two kinds of collector grains was found with the more polar polymers (metasilicate and alginate). The trend in sticking coefficients was correlated with the surface energy of the polymer-modified iron surface as measured by the static contact angle method. From these data one can conclude that the hydrophobicity of the polymer dispersant is a key factor in targeting zerovalent iron to DNAPL source zones in soil and groundwater.

Introduction

Nanoscale zerovalent iron is being increasingly studied and tested for the *in situ* remediation of contaminated soil and groundwater sites that contain dense nonaqueous phase liquids (DNAPLs) (1–7). DNAPLs exist in the subsurface environment in a variety of forms, including hydrophobic liquid droplets (or “ganglia”) that equilibrate very slowly with the groundwater because of low solubility (8, 9). Because the

volume of soil and groundwater that can be contaminated by relatively small amounts of DNAPLs is very large, laboratory and field studies of *in situ* remediation typically involve a very large stoichiometric excess of iron, and this increases the cost and environmental impact of the remediation (10–18). The efficient delivery of zerovalent iron particles - as well as other kinds of *in situ* remediants, such as sorbents and oxidizing agents - to dispersed contamination sources in soil and groundwater is thus an important practical problem.

Iron nanoparticles, which are more reactive than iron filings or microparticles, are efficiently filtered in saturated granular media such as soils. In order to improve the transport of nanoiron, particle “delivery vehicles”, including microemulsions (19, 20), adsorbed anionic synthetic polymers and biopolymers (21–31), anionic carbons (21, 32), silica (33), and multifunctional triblock copolymers (28, 29, 34) have been studied. It is now well established that anionic polymers impede particle aggregation and dramatically lower the probability that collisions between the particles and soil surfaces result in adhesion (30, 35). This sticking coefficient (or probability) (α) has been calculated using classical filtration theory for various model soils from column transport studies.

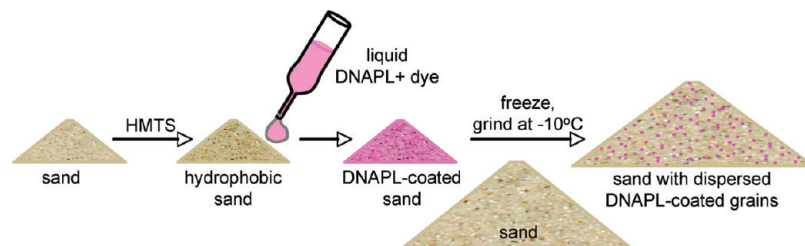
Lowry and co-workers introduced the concept of targeting nanoparticles to contaminants in their studies of iron nanoparticles with an adsorbed triblock copolymer layer (28). They found that the particles localized at the interface between liquid trichloroethylene and water and that the oil-in-water emulsions so formed were stable over periods of months. They attributed this behavior to the triblock copolymer’s ability to rearrange in different environments, specifically to expose the hydrophobic polystyrene block when in contact with DNAPLs. Similar behavior has more recently been found by Zhan et al., who studied carbon microspheres containing nanoiron and stabilized by carboxymethylcellulose (36). While these results are promising, the partitioning experiment does not quantify targeting in the sense of particle transport behavior.

Both triblock copolymers and the borohydride reagent used by Zhan et al. to prepare carbon/nanoiron microspheres are too expensive to use in the quantities needed for full-scale environmental remediation projects, which can involve thousands of kilograms of iron. For these applications, natural or synthetic homopolymers or biopolymers are typically used in conjunction with iron nanoparticles. It is thus relevant to ask whether these simpler materials can target contaminants effectively. Studies of capillary interactions, carried out in a very different context, have shown that colloidal particles tend to localize at liquid–liquid interfaces when the energy of the two contacting liquids ($\gamma_{L1,L2}$) is large compared to the difference between the energies of the two particle–liquid interfaces ($|\gamma_{p,L1} - \gamma_{p,L2}|$) (37). This principle has been used to spontaneously assemble ternary systems of oil, water, and particles into colloidosomes, which contain a densely packed layer of particles at the liquid–liquid interface (38). These observations in other colloidal systems suggest that iron particle targeting to liquid–liquid (DNAPL–water) or liquid–solid (DNAPL–soil) interfaces could be quite effective with simple homopolymers. In the case of a high energy liquid–liquid interface, such as DNAPLs and water, one should expect particles with a broad range of moderately hydrophobic polymer coatings to adhere spontaneously to the interface.

In this paper, we test this hypothesis by using micrometer-size, spherical iron particles, coated with hydrophilic and moderately hydrophobic anionic polymers. Microiron was

* Corresponding author phone: (814)863-9637; fax: (814)863-8403; e-mail: tem5@psu.edu.

SCHEME 1. Process Flow for Preparing Well-Dispersed Mixtures of Sand and Dye-Tagged DNAPL-Coated Sand Grains^a



^a HTMS-modified sand grains were coated with a thin layer of dichlorobenzene, which was frozen for mixing with unmodified sand.

chosen for this study because its transport properties in water-saturated sand columns have been well studied and modeled quantitatively (30). In our earlier studies with these particles, we examined the distribution of particle sizes before and after elution through sand columns. These studies were carried out at low particle number density ($\sim 4 \times 10^8/\text{cm}^3$) and in the presence of anionic polyelectrolytes in order to inhibit aggregation. From the profiles of retained iron in the columns, we were able to quantify the deviation of the filtration data from classical filtration theory (CFT) and to obtain average sticking coefficients for the iron microparticles (30). Here, we extend this method in order to estimate the sticking coefficients of iron microparticles at unmodified and chlorobenzene-modified sand grains. The DNAPL sticking coefficients of particles modified with different anionic homopolymers are then correlated with their surface energies, measured by the static contact angle method. This correlation is useful for selecting anionic polymers that target particles to DNAPL contaminants, i.e., polymers that impart a low sticking coefficient for polar, unmodified sand grains but a high sticking coefficient for DNAPLs.

Results and Discussion

Preparation of DNAPL-Loaded Sand Columns. The approach taken here to quantifying the targeting of iron particles to contaminants involves analysis of the elution behavior of micrometer-size iron particles in water-saturated sand columns that contain a small fraction of DNAPL-coated grains. While the transport of bacteria in DNAPL-contaminated columns has been studied before, it was not possible to obtain quantitative sticking coefficients because inhomogeneously distributed contaminant droplets modified the pattern of flow in the columns (39). Quantitative filtration models generally assume a single collector size and a uniform pore velocity. Thus, it was important to devise a method for dispersing hydrophobic DNAPL-coated sand grains in water-saturated sand columns in such a way that the hydrophobic grains would not coalesce into larger aggregates.

This problem was solved using the process flow sketched in Scheme 1. In order to maintain a single collector diameter, $160 \pm 45 \mu\text{m}$ diameter sand particles were modified with a hydrophobic silane monolayer (hexadecyltrimethoxysilane) to which a thin ($\sim 8 \mu\text{m}$) coating of dichlorobenzene containing a porphyrin dye was applied. The modified grains were then dispersed at 5–10% loading in unmodified sand. By using a mixture of dichlorobenzene isomers that was solid at the mixing temperature (-10°C), it was possible to prevent agglomeration of the dichlorobenzene-coated grains. Figure 1 shows an optical microscope image of a 5% sand mixture in both bright field and fluorescence modes. The DNAPL-modified sand grain that is brighter than the surrounding particles in the fluorescence image is surrounded by unmodified sand grains.

Measurements of Iron Microparticle Elution and Retention. Columns were loaded with the physical mixture of sand and DNAPL-coated hydrophobic sand, in which the

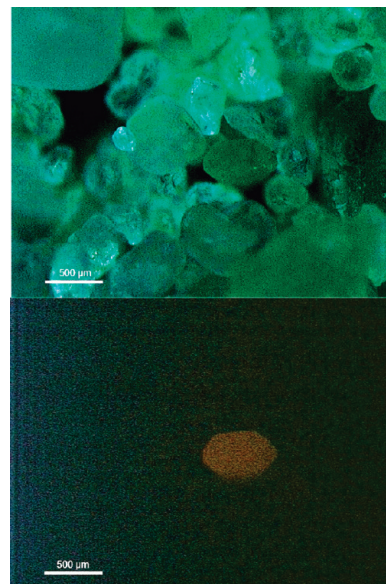


FIGURE 1. Contrast-enhanced optical microscope images of a sand mixture containing 95% sand and 5% dichlorobenzene-coated sand grains. The dichlorobenzene layer was stained with fluorescent meso-tetraphenylporphine. Top: bright field image. Bottom: fluorescence image of the same area.

DNAPL coating was kept frozen to prevent particle aggregation. These sand-packed columns were allowed to warm to ambient temperature (where the dichlorobenzene mixture on the dispersed hydrophobic grains liquefied) and were then rinsed with water before loading with polymer-coated CIP iron. The combined amount of dichlorobenzene eluted in the processes of packing/rinsing the column and eluting polymer-coated CIP, as determined by UV-visible spectroscopy, was about 4% of the total, meaning that 96% remained on the hydrophobic grains.

BASF-HQ carbonyl iron powder, which was used in the column transport experiments, consists of spherical particles with a log-normal distribution of diameters (d_0) peaked at $0.9 \mu\text{m}$. The particle size distribution, composition, and surface chemical properties of this material have been described in a previous paper (30). Figure 2 shows profiles of iron retained by sand and contaminated sand columns when these microparticles were modified with carboxymethylcellulose (CMC) and eluted with water. Except for the fact that the iron is more strongly retained in the lower part of the contaminated column, the elution profiles are similar in shape. Similar profiles were observed previously for microiron coated with polyacrylate (PAA) (30), where it was found that the largest particles in the distribution were selectively filtered near the top of the column.

Below about 7 cm depth in the columns, the iron retention profiles in Figure 2 are close to the prediction of the Tufenkji-Elimelech model (TE) for particle filtration in the clean-bed limit (40). The TE model, like earlier models (41), is based

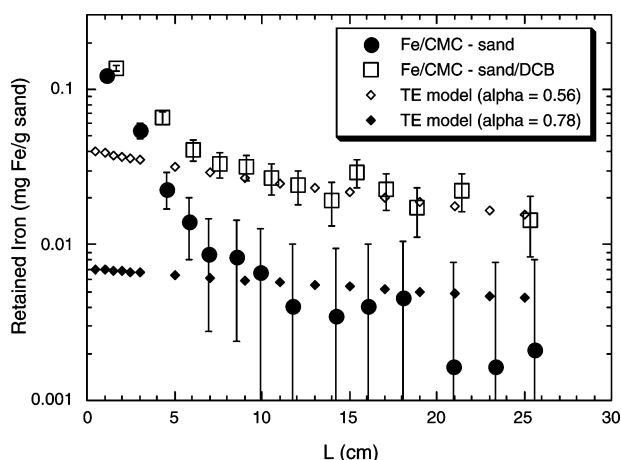


FIGURE 2. Profiles of retained microiron particles in water-saturated sand and mixed columns containing 5% contaminated sand grains. Ten mg of iron and 2 mg of CMC were injected in 2 mL of water and eluted with 200 mL of water. Fits to the TE model, with sticking coefficients of 0.78 and 0.56 for the sand and mixed columns, are shown.

on classical filtration theory (CFT) in the sense that the collection of mobile particles by sand grains is a first-order kinetic process. CFT predicts that the profile of retained iron should decrease approximately exponentially with depth in the column. The deviation from CFT observed at the top of the columns can be understood as the selective capture of larger particles, as explained in a subsequent paper by Tufenji and Elimelech (42). This behavior has now been observed in a number of filtration experiments that involve a distribution of sizes of the mobile particles (30–45).

Because sticking coefficients calculated from elution data using the TE model provide reasonable fits to the particle retention profiles in the lower parts of these columns, the model can be used to compare sticking coefficients for the contaminated and uncontaminated sand grains. It is clear from Figure 2 that a single sticking coefficient does not describe the behavior of the entire distribution of iron particle sizes. Nevertheless, the ratio of sticking coefficients is a relatively model-independent quantity and the derived values change by only a few percent when the Rajagopalan-Tien (RT) model (41) is used in place of the TE model.

In the TE and RT models, which are first-order kinetic models for particle filtration, the number density (N) of particles in the mobile phase at the end of a column at length L is given by eq 1. Here N_0 is the number density of particles in the unfiltered suspension and the product

$$\ln\left(\frac{N}{N_0}\right) = -\alpha L \quad (1)$$

$$\lambda = \frac{3}{2d_c}(1 - \theta)\eta \quad (2)$$

$$\eta = \eta_D + \eta_I + \eta_G \quad (3)$$

$(\alpha\lambda)^{-1}$ is a filtration length (46). In the clean bed limit, the parameter λ depends on the column porosity θ , the collector diameter d_c , and the collection efficiency η , according to eq 2. η is in turn the sum (eq 3) of contributions from diffusion (η_D), interception (η_I), and sedimentation (η_G) capture mechanisms, which depend primarily on the particle and collector diameters, column porosity, particle specific gravity, and pore velocity. An additional dependence of η on the Hamaker constant of the particles and collectors is taken into account in the TE model (40). For the purposes of this analysis, a single Hamaker constant (1×10^{-20} J) was used

TABLE 1. Mass Fraction of Iron Particles Eluted and Calculated Sticking Coefficients^a

polymer	mass fraction iron eluted		α_{sand}	α_{eff}	α_{DNAPL}
	sand column	mixed column			
PAA	0.91 ± 0.03	0.80 ± 0.01	0.0043	0.011	0.13
CMC	0.78 ± 0.01	0.56 ± 0.03	0.012	0.032	0.40
SMS	0.56 ± 0.02	0.58 ± 0.02	0.032	0.029	—
ALG	0.46 ± 0.02	0.48 ± 0.02	0.045	0.042	—

^a Error bars indicate the standard deviation of the mean, based on replicate measurements. Mixed columns contained 5% modified sand grains. PAA = sodium poly(acrylate), CMC = sodium carboxymethylcellulose, SMS = sodium metasilicate, ALG = sodium alginate.

for both the modified and unmodified sand grains and variation by a factor of 2 had little effect ($\sim 10\%$) on the derived values of α . λ values were calculated over the range of iron particle sizes in the distribution, and their contributions were added to calculate the mass fraction of eluted iron. Values of α were obtained by constraining the calculation to match the experimentally determined mass fraction of eluted iron (30).

For a mixed column containing two collectors with the same d_c , first-order models predict that the collection rates are additive, and the rate constants are proportional to α for the two kinds of collectors. In this case eq 1 can be replaced by eq 4 in which χ is the fraction of the modified grains, α_{sand} is the sticking coefficient for the unmodified sand grains

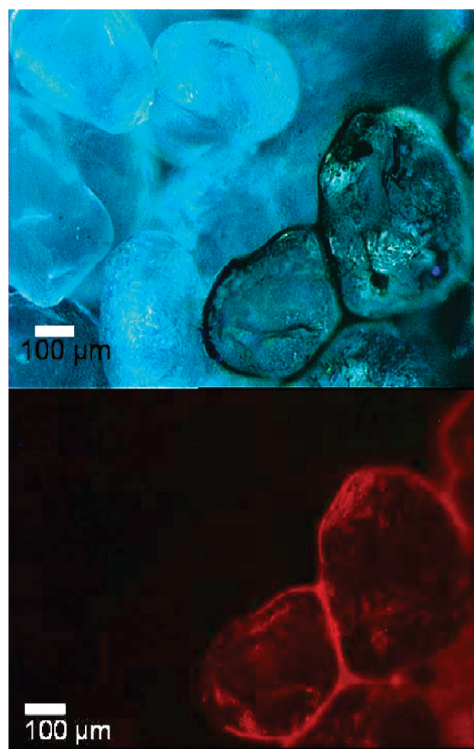


FIGURE 3. Bright field and fluorescence microscope images of sand particles obtained from contaminated columns eluted with iron/CMC suspensions. In the top image, iron particles appear as a dark outline around the sand grains at the right. The same grains show the dye/DNAPL coating in the fluorescence image (bottom).

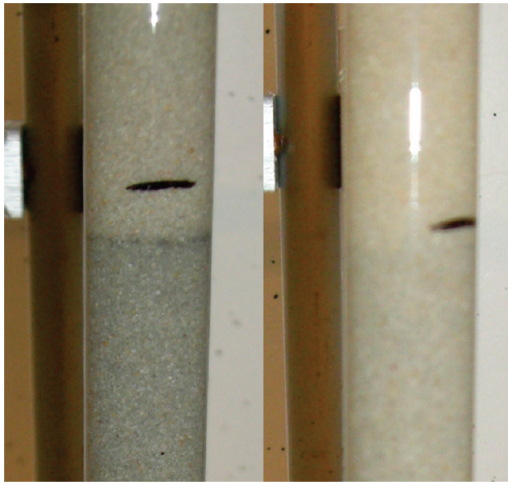


FIGURE 4. Sand columns after elution of 2.00 g of iron in 400 mL of CMC (left) and SMS (right) solutions. The black line initially marked the boundary between uncontaminated sand and 90% sand/10% DNAPL-coated sand, which shifted downward as the sand settled. The contrast between the uncontaminated and contaminated sections is more clearly visible in the CMC column.

$$\ln\left(\frac{N}{N_0}\right) = -(1 - \chi)\alpha_{\text{sand}} + \chi\alpha_{\text{DNAPL}}\lambda L \quad (4)$$

and α_{DNAPL} is the sticking coefficient for grains coated with dichlorobenzene. The quantity in square brackets is an effective sticking coefficient (α_{eff}), which can be obtained by fitting elution data to either the RT or TE models. By comparing α_{eff} for mixed columns with α_{sand} obtained with pure sand columns, α_{DNAPL} values were obtained for four homopolymers. These results (TE model) are summarized in Table 1.

Table 1 shows that for iron particles with adsorbed layers of PAA and CMC, α_{DNAPL} values are approximately 30 times larger than α_{sand} , indicating a strong affinity for the DNAPL surface. In contrast, within experimental error there was no difference between α_{sand} and α_{eff} for iron particles modified with the more polar SMS or ALG polymers.

Microscopic analysis of particles from mixed columns (Figure 3) confirms that iron particles are localized to the contaminated grains. Another visual demonstration of the sharp contrast between particle retention by contaminated and uncontaminated sand can be obtained with layered columns, as shown in Figure 4. In this experiment, iron particles coated with CMC are preferentially retained in the lower, contaminated part of the column, despite the fact that the eluted particle concentration N (with a single collector) should decay exponentially with distance from the top of the column. In the case of the SMS polymer, there is much less visible contrast between the amount of iron retained in the contaminated and uncontaminated parts of the column.

Contact Angle Measurements of Iron Particle Surface

Energy. Lowry and co-workers have shown that at the concentrations used in the elution experiments described above, CMC and other anionic polymers adsorb strongly to the iron surface at saturation loadings in the $2-3 \times 10^{-9}$ monomer unit/cm² range, suggesting a looped monolayer arrangement of polymer chains (47). At this loading, the polymer can be expected to strongly influence the surface energy (γ) of particles to which it is adsorbed. The surface energies of iron microparticles with adsorbed polymer layers were estimated from contact angle data. Static contact angles were measured with three polar fluids - water, ethylene glycol, and formamide - and are shown in Table 2. Attempts to measure contact angles with less polar fluids were unsuccessful because those solvents swelled or dissolved the adhesive that held the iron particles to the glass slides on which the contact angles were measured.

The surface tension of each iron surface was calculated using eq 5 (48)

$$\gamma_L(1 + \cos \theta_{\text{SL}}) = 2(\sqrt{\gamma_s^d \gamma_L^d} + \sqrt{\gamma_s^p \gamma_L^p} + \sqrt{\gamma_s^h \gamma_L^h}) \quad (5)$$

Here γ_L is the liquid surface tension; γ_L^d , γ_L^p , and γ_L^h are the liquid surface tension components due to dispersion, polar, and hydrogen-bonding forces, respectively; θ_{SL} is the contact angle of the liquid with the solid surface; and γ_s^d , γ_s^p , and γ_s^h are the solid surface tension components due to dispersion, polar, and hydrogen-bonding forces, respectively. It is assumed that the surface tension of the solid is approximated well by γ_{sv} in the presence of the vapor (in this case air) used in the measurement. Contact angles were measured for three different liquids, and three equations are generated

$$\gamma_{\text{L,water}}(1 + \cos \theta_{\text{SL,water}}) = 2(\sqrt{\gamma_s^d \gamma_{\text{L,water}}^d} + \sqrt{\gamma_s^p \gamma_{\text{L,water}}^p} + \sqrt{\gamma_s^h \gamma_{\text{L,water}}^h}) \quad (6)$$

$$\gamma_{\text{L,glycol}}(1 + \cos \theta_{\text{SL,glycol}}) = 2(\sqrt{\gamma_s^d \gamma_{\text{L,glycol}}^d} + \sqrt{\gamma_s^p \gamma_{\text{L,glycol}}^p} + \sqrt{\gamma_s^h \gamma_{\text{L,glycol}}^h}) \quad (7)$$

$$\gamma_{\text{L,form}}(1 + \cos \theta_{\text{SL,form}}) = 2(\sqrt{\gamma_s^d \gamma_{\text{L,form}}^d} + \sqrt{\gamma_s^p \gamma_{\text{L,form}}^p} + \sqrt{\gamma_s^h \gamma_{\text{L,form}}^h}) \quad (8)$$

For each polymer-coated iron surface, contact angles of the three liquids were measured, providing the θ terms on the left side of eqs 6–8 for the sample. The total surface tension and component values have been previously reported for each of the three liquids, and thus each of the γ_L terms is known (49). This gives for each surface three equations in three unknowns ($(\gamma_s^d)^{1/2}$, $(\gamma_s^p)^{1/2}$, and $(\gamma_s^h)^{1/2}$), which can be solved to calculate the solid surface tension components of the polymer-coated iron particles. The values obtained were squared to give γ_s^d , γ_s^p , and γ_s^h , respectively. These components were then summed to obtain the total solid powder surface tension γ_s for a given iron particle surface (Table 2).

TABLE 2. Contact Angle (θ) Data and Calculated Surface Energies of Polymer-Coated Iron Particles

	PAA	CMC	SMS	ALG	unmodified iron
γ (deg) - water	63.9 ± 1.6	50.7 ± 5.3	~0	~0	30.3 ± 2.3
γ (deg) - ethylene glycol	55.5 ± 1.7	43.9 ± 3.6	11.2 ± 1.0	~0	18.8 ± 1.7
γ (deg) - formamide	40.8 ± 2.9	33.3 ± 3.4	~0	~0	38.3 ± 2.5
γ_s^d (mN/m)	12.7 ± 0.9	5.0 ± 0.9	0 (estimate)	0 (estimate)	0.1 ± 0.0
γ_s^p (mN/m)	10.0 ± 0.8	33.7 ± 2.4	43 (estimate)	41 (estimate)	24.2 ± 0.8
γ_s^h (mN/m)	16.3 ± 1.0	14.7 ± 1.6	42 (estimate)	43 (estimate)	47.4 ± 1.1
γ_s^{tot} (mN/m)	39.0 ± 1.6	53.4 ± 3.0	85 (estimate)	84 (estimate)	71.6 ± 1.4

In the case of the polar polymers (SMS and ALG), contact angles were too low to measure with polar fluids, i.e., the drops spread completely on the surface. It is important to note that the unmodified iron powder sample used as a control sample gave measurable contact angles with these fluids. Thus one can conclude that the wetting observed with SMS and ALG is a result of polymer adsorption on the surface.

The estimates of the different components of the surface tension show that the polar and hydrogen bonding components dominate the surface energy of SMS- and ALG-coated iron, as expected from the high charge density of these polymers. It is important to note that the energies calculated for SMS- and ALG-coated surfaces are rough estimates, obtained by using 0 values for contact angles where indicated in Table 2. One can conclude nevertheless that these are high energy surfaces because they are completely wetted by water. In contrast, the PAA- and CMC-coated iron surfaces gave significantly lower total surface energies.

Correlation of α_{DNAPL} Values with Iron Particle Surface Energy. For the anionic homopolymers studied here, there is a clear trend between particle surface energy (Table 2) and the α_{DNAPL} values obtained from transport data (Table 1). Polymers that gave low water contact angles (SMS and ALG) did not result in measurable DNAPL targeting, whereas the more hydrophobic polymers (PAA and CMC) had much higher α_{DNAPL} values, with $\alpha_{\text{DNAPL}}/\alpha_{\text{sand}} \approx 30$ for both PAA and CMC. This trend is consistent with the hypothesis that targeting is driven by lowering the total interfacial energy (37, 38), because the surface tensions of PAA- and CMC-coated iron surfaces are intermediate between those of water ($\gamma_{\text{water}} = 72.8 \text{ mN/m}$) and m-dichlorobenzene (35.4 mN/m) (50). The latter is in the range of many environmentally relevant DNAPL contaminants, and it thus serves as a good model for the purpose of evaluating polymers for targeting.

The trend observed with the four polymers studied here suggests that the best polymer adsorbates for the *in situ* remediation of DNAPLs by iron particles - i.e., those that impart high α_{DNAPL} values - should be moderately hydrophobic. Ideally, one would like to identify anionic polymers or other support materials that can approach α_{DNAPL} values of 1.0 while maintaining a low sticking coefficient to soil surfaces under realistic conditions of flow and ionic strength. Both the electrostatic and electrosteric properties of polymer coatings contribute to particle sticking coefficients (34, 35). With unmodified sand columns, we found a correlation between sticking coefficient and particle zeta potential and used this to minimize α for different polyelectrolytes and mixtures. The data in Table 1 show that particles with similar α_{sand} values can have very different effectiveness in targeting, as expressed by the $\alpha_{\text{DNAPL}}/\alpha_{\text{sand}}$ ratio. This ratio depends strongly on the polymer surface energy, which is determined primarily by the polymer charge density and the density of hydrogen bonding donor/acceptor groups. In principle, these are separately adjustable structural parameters of the polymer. The best polymers should minimize particle adhesion to polar surfaces through energetically and entropically driven electrosteric interactions (repulsion of like charges, random coiling of polymer main chains and side chains) and should target DNAPL surfaces by minimizing the energy of the DNAPL/water interface.

The methods described here should be useful for obtaining estimates of nanoparticle surface energies and for correlating them with transport in contaminated and uncontaminated soils. This information can be used to design support materials for targeting of iron nanoparticles, which are more relevant to *in situ* remediation than the spherical microparticles that we have used as a model in this study. Because the surface energy effect should apply generally to particle adhesion, for practical applications it will also be important to quantify the extent to which soil organic matter and other

low surface energy components of real soils affect the targeting of nanoiron. Experiments along these lines are currently in progress.

Acknowledgments

This work was supported by the National Science Foundation under grant CHE-0910513.

Supporting Information Available

Experimental details for materials, transport experiments, and contact angle measurements. This material is available free of charge via the Internet at <http://pubs.acs.org>.

Literature Cited

- Gillham, R. W.; O'Hannesin, S. F. Enhanced degradation of halogenated aliphatics by zero-valent iron. *Ground Water* **1994**, *32*, 958-967.
- Matheson, L. J.; Tratnyek, P. G. Reductive dehalogenation of chlorinated methanes by iron metal. *Environ. Sci. Technol.* **1994**, *28*, 2045-2053.
- Roberts, A. L.; Totten, L. A.; Arnold, W. A.; Burris, D. R.; Campbell, T. J. Reductive elimination of chlorinated ethylenes by zero-valent metals. *Environ. Sci. Technol.* **1996**, *30*, 2654-2659.
- Tratnyek, P. G.; Johnson, T. L.; Scherer, M. M.; Eykholt, G. R. Remediating ground water with zero-valent metals: chemical considerations in barrier design. *Ground Water Monit. Rem. Winter* **1997**, 108-114.
- Liang, L.; Korte, N.; Goodlaxson, J. D.; Clausen, J.; Fernando, Q.; Muftikian, R. Byproduct formation during the reduction of TCE by zero-valence iron and palladized iron. *Ground Water Monit. Rem. Winter* **1997**, 122-127.
- Blowes, D. W.; Ptacek, C. J.; Jambor, J. L. In-Situ Remediation of Cr(VI)-Contaminated groundwater using permeable reactive walls: laboratory studies. *Environ. Sci. Technol.* **1997**, *31*, 3348-3357.
- Powell, R. M.; Puls, R. W.; Hightower, S. K.; Sabatini, D. A. Coupled iron corrosion and chromate reduction: mechanisms for subsurface remediation. *Environ. Sci. Technol.* **1995**, *29*, 1913-1922.
- Luthy, R. G.; Aiken, G. R.; Brusseau, M. L.; Cunningham, S. D.; Gschwend, P. M.; Pignatello, J. J.; Reinhard, M.; Traina, S. J.; Weber, W. J., Jr.; Westall, J. C. Sequestration of hydrophobic organic contaminants by geosorbents. *Environ. Sci. Technol.* **1997**, *31*, 3341-3347.
- Zhang, W.; Bouwer, E.; Ball, W. Bioavailability of hydrophobic organic contaminants: effects and implications of sorption-related mass transfer on bioremediation. *Ground Water Monit. Rem.* **1998**, 126-138, Winter.
- Zhang, W. X. Nanoscale iron particles for environmental remediation: an overview. *J. Nanoparticle Res.* **2003**, *5*, 323-332.
- Boronina, T.; Klabunde, K. J.; Sergeev, G. Destruction of organohalides in water using metal particles: carbon tetrachloride/water reactions with magnesium, tin, and zinc. *Environ. Sci. Technol.* **1995**, *29*, 1511-1517.
- Wang, C.-B.; Zhang, W.-X. Synthesizing nanoscale iron particles for rapid and complete dechlorination of TCE and PCBs. *Environ. Sci. Technol.* **1997**, *31* (7), 2154-2156.
- Kaplan, D. I.; Cantrell, K. J.; Wietsma, T. J.; Potter, M. A. Retention of zero-valent iron colloids by sand columns: application to chemical barrier formation. *J. Environ. Qual.* **1996**, *25*, 1086-1094.
- Ponder, S. M.; Darab, J. G.; Mallouk, T. E. Remediation of Cr(VI) and Pb(II) aqueous solutions using supported, nanoscale zero-valent iron. *Environ. Sci. Technol.* **2000**, *34*, 2564-2569.
- Elliott, D. W.; Zhang, W.-X. Field assessment of nanoscale bimetallic particles for groundwater treatment. *Environ. Sci. Technol.* **2001**, *35*, 4922-4926.
- Schrick, B.; Blough, J. L.; Jones, A. D.; Mallouk, T. E. Hydrodechlorination of trichloroethylene to hydrocarbons using bimetallic nickel-iron nanoparticles. *Chem. Mater.* **2002**, *14*, 5140-5147.
- Liu, Y. Q.; Majetich, S. A.; Tilton, R. D.; Sholl, D. S.; Lowry, G. V. TCE dechlorination rates, pathways, and efficiency of nanoscale iron particles with different properties. *Environ. Sci. Technol.* **2005**, *39*, 1338-1345.
- Varadhi, S. N.; Gill, H. S.; Apoldo, L. J.; Liao, K.; Blackman, R. A.; Wittman, W. K. Full-scale nanoiron injection for treatment of

- groundwater contaminated with chlorinated hydrocarbons, Natural Gas Technologies 2005 Conference, Orlando, FL (February 2005).
- (19) Quinn, J.; Geiger, C.; Clausen, C.; Brooks, K.; Coon, C.; O'Hara, S.; Krug, T.; Major, D.; Yoon, W.-S.; Gavaskar, A.; Holdsworth, T. Field demonstration of DNAPL dehalogenation using emulsified zero-valent iron. *Environ. Sci. Technol.* **2005**, *39*, 1309–1318.
 - (20) Berge, N. D.; Ramsburg, A. Oil-in-water emulsions for encapsulated delivery of reactive iron particles, *Environ. Sci. Technol.* **2009**, *43*, 5060–5066.
 - (21) Schrick, B.; Hydutsky, B. W.; Blough, J. L.; Mallouk, T. E. Delivery vehicles for zerovalent metal nanoparticles in soil and groundwater. *Chem. Mater.* **2004**, *16*, 2187–2193.
 - (22) He, F.; Zhao, D. Preparation and characterization of a new class of starch-stabilized bimetallic nanoparticles for degradation of chlorinated hydrocarbons in water. *Environ. Sci. Technol.* **2005**, *39*, 3314–3320.
 - (23) He, F.; Zhao, D. Manipulating the size and dispersability of zerovalent iron nanoparticles by use of carboxymethylcellulose stabilizers. *Environ. Sci. Technol.* **2007**, *41*, 6216–6221.
 - (24) He, F.; Zhao, D.; Liu, J.; Roberts, C. B. Stabilization of Fe-Pd nanoparticles with sodium carboxymethyl cellulose for enhanced transport and dechlorination of trichloroethylene in soil and groundwater. *Ind. Eng. Chem. Res.* **2007**, *46*, 29–34.
 - (25) Vecchia, E. D.; Luna, M.; Sethi, R. Transport in porous media of highly concentrated iron micro and nanoparticles in the presence of xanthan gum. *Environ. Sci. Technol.* **2009**, *43*, 8942–8947.
 - (26) Tiraferri, A.; Chen, K. L.; Sethi, R.; Elimelech, M. Reduced aggregation and sedimentation of zero-valent iron nanoparticles in the presence of guar gum. *J. Colloid Interface Sci.* **2008**, *324*, 71–79.
 - (27) Tiraferri, A.; Sethi, R. Enhanced transport of zerovalent iron nanoparticles in saturated porous media by guar gum. *J. Nanopart. Res.* **2009**, *11*, 635–645.
 - (28) Saleh, N.; Phenrat, T.; Sirk, K.; Dufour, B.; Ok, J.; Sarbu, T.; Matyjaszewski, K.; Tilton, R. D.; Lowry, G. V. Adsorbed triblock copolymers deliver reactive iron nanoparticles to the oil/water interface. *Nano Lett.* **2005**, *5*, 2489.
 - (29) Saleh, N.; Sirk, K.; Liu, Y.; Phenrat, T.; Dufour, B.; Matyjaszewski, K.; Tilton, R. D.; Lowry, G. V. Surface modifications enhance nanoiron transport and NAPL targeting in saturated porous media. *Environ. Eng. Sci.* **2007**, *24*, 45–57.
 - (30) Hydutsky, B. W.; Mack, E. J.; Beckerman, B. B.; Skluzacek, J. M.; Mallouk, T. E. Optimization of nano- and micro-iron transport through sand columns using polyelectrolyte mixtures. *Environ. Sci. Technol.* **2007**, *41*, 6418–6424.
 - (31) Kanel, S. R.; Choi, H. The transport characteristics of polymer stabilized nano scale zero-valent iron in porous media. *Water Sci. Technol.* **2007**, *55*, 157–162.
 - (32) Hoch, L. B.; Mack, E. J.; Hydutsky, B. W.; Hershman, J. M.; Mallouk, T. E. Carbothermal synthesis of carbon-supported nanoscale zero-valent iron particles for the remediation of hexavalent chromium. *Environ. Sci. Technol.* **2008**, *42*, 2600–2605.
 - (33) Zhan, J.; Zheng, T.; Piringner, G.; Day, C.; McPherson, G. L.; Lu, Y.; Papadopoulos, K.; John, V. T. Transport characteristics of nanoscale functional zerovalent iron/silica composites for in situ remediation of trichloroethylene. *Environ. Sci. Technol.* **2008**, *42*, 8871–8876.
 - (34) Saleh, N.; Kim, H.-J.; Phenrat, T.; Matyjaszewski, K.; Tilton, R. D.; Lowry, G. D. Ionic strength and composition affect the mobility of surface-modified Fe⁰ nanoparticles in water-saturated sand columns. *Environ. Sci. Technol.* **2008**, *42*, 3349–3355.
 - (35) Sirk, K. M.; Saleh, N. B.; Phenrat, T.; Kim, H.-J.; Dufour, B.; Ok, J.; Golas, P. L.; Matyjaszewski, K.; Lowry, G. V.; Tilton, R. D. Effect of adsorbed polyelectrolytes on nanoscale zero valent iron particle attachment to soil surface models. *Environ. Sci. Technol.* **2009**, *43*, 3803–3808.
 - (36) Zhan, J.; Sunkara, B.; Le, L.; John, V. T.; He, J.; McPherson, G. L.; Piringner, G.; Lu, Y. Multifunctional colloidal particles for in situ remediation of chlorinated hydrocarbons. *Environ. Sci. Technol.* **2009**, *43*, 8616–8621.
 - (37) Kralchevsky, P. A.; Nagayama, K. Capillary interactions between particles bound to interfaces, liquid films and biomembranes. *Adv. Colloid Interface Sci.* **2000**, *85*, 145–192.
 - (38) Dinsmore, A. D.; Hsu, M. F.; Nikolaidis, M. G.; Marquez, M.; Bausch, A. R.; Weitz, D. A. Colloidosomes: selectively permeable capsules composed of colloidal particles. *Science* **2002**, *298*, 1006–1009.
 - (39) Rogers, B.; Logan, B. E. Bacterial transport in NAPL-contaminated porous media. *J. Environ. Eng.* **2000**, 657–666.
 - (40) Tufenkji, N.; Elimelech, M. Correlation equation for predicting single-collector efficiency in physicochemical filtration in saturated porous media. *Environ. Sci. Technol.* **2004**, *38*, 529–539.
 - (41) Rajagopalan, R.; Tien, C. Trajectory analysis of deep-bed filtration with the sphere-in-cell porous media model. *AIChE J.* **1976**, *22*, 523–33.
 - (42) Tufenkji, N.; Elimelech, M. Breakdown of colloid filtration theory: role of the secondary energy minimum and surface charge heterogeneities. *Langmuir* **2005**, *21*, 841–852.
 - (43) (a) Tong, M.; Johnson, W. P. Excess colloid retention in porous media as a function of colloid size, fluid velocity, and grain angularity. *Environ. Sci. Technol.* **2006**, *40*, 7725–7731.
 - (44) Tong, M.; Johnson, W. P. Colloid population heterogeneity drives hyperexponential deviation from classic filtration theory. *Environ. Sci. Technol.* **2007**, *41*, 493–499.
 - (45) Sharma, P.; Flury, M.; Mattson, E. D. Studying colloid transport in porous media using a geocentrifuge. *Water Resour. Res.* **2008**, *44*, W07407.
 - (46) Yao, K.-M.; Habibian, M. T.; O'Melia, C. R. Water and waste water filtration. Concepts and applications. *Environ. Sci. Technol.* **1971**, *5*, 1105–1112.
 - (47) Phenrat, T.; Liu, Y.; Tilton, R.; Lowry, G. V. Adsorbed polyelectrolyte coatings decrease Fe⁰ nanoparticle reactivity with TCE in water: conceptual model and mechanisms. *Environ. Sci. Technol.* **2009**, *43*, 1507.
 - (48) Hozumi, A.; Asakura, S.; Fuwa, A.; Shirahata, N.; Kameyama, T. Preparation of a well-defined amino-terminated self-assembled monolayer and copper microlines on a polyimide substrate covered with an oxide nanoskin. *Langmuir* **2005**, *21*, 8234–8242.
 - (49) Panzer, J. Components of solid surface free energy from wetting measurements. *J. Colloid Interface Sci.* **1973**, *44*, 142–161.
 - (50) *CRC Handbook of Chemistry and Physics*, 84th ed.; Lide, D. R., Ed.; CRC Press: Boca Raton, FL, 2003; pp 6–150–152.

ES1017398